ISSN: 2754-4753

Journal of Physics & Optics Sciences

SCIENTIFIC Research and Community

Review Article

Open Access

The Fiberglass Genetic Study, Structural and Optical Transmission

Abodunrin OW

Department of Mathematical and Physical Sciences, Afe Babalola University, Ekiti, State, Nigeria

ABSTRACT

The four compositional samples were investigated in the high thermal resistance domain of fiberglass through the classical melt-quenching technique at temperatures up to 1500 °C. The analyses of the samples were carried out using thermal expansion, hydrolytic stability, density, Ultraviolet-visible (UV-Vis) transmission, and X-ray diffraction. The hydrolytic stability of the analyzed samples showed that they are chemically stable. From the thermal expansion. The examined samples had low expansion coefficients. On the UV-V transmittance, glasses have notable transmittances in the ultraviolet region down to 250 nm. Proton Induce X-Ray Emission (PIXE) and Rutherford Back Scattering (RBS) were used to depict the elemental compositions of glass samples. The Scanning Electron microscope (SEM) was used to examine the morphology of the glass samples. The presence of broad band in the glass samples in the X-ray analyses showed the amorphous nature of the glass contents. The presence of a specific high-frequency distinct peak in the spectrum showed that the fiberglass samples did not crystallize.

***Corresponding author**

Abodunrin OW, Department of Mathematical and Physical Sciences, Afe Babalola University, Ekiti, State, Nigeria.

Received: November 12, 2025; **Accepted:** November 18, 2025; **Published:** January 20, 2026

Keywords: Fiberglass, UV-Vis Transmission, Prospective Applications

Introduction

Fiberglass has low thermal expansion, high chemical durability, and high electrical resistivity [1]. These properties make them suitable for various scientific and industrial applications, such as laboratory glassware, lighting, and electronics [1]. One emerging application of fiberglass is in boat building, chemical industries, turbine blades, mesh fabrics, and construction industries [2]. Fiberglass is a good candidate for light wave applications because they have high transmittance of UV radiation. Fiberglass also has high resistance to UV-induced degradation, which means they maintain their mechanical and optical properties even after prolonged exposure to UVC radiation [1,2]. This ensures that the glass material does not crack, or lose its transparency over time. Moreover, fiberglass has high thermal shock resistance, which means they can withstand rapid changes in temperature without breaking points or cracking units and at the same time transmit light signals. This is important for light-sound wave devices that may operate at high temperatures. They experience frequent on-off cycles [3] revealed the connectivity between the content of Al_2O_3 and SiO_2 and the effects on the units of glass structure, and interconnectivity. These have effects on the units of glass structure and the chemical stability and the UV transmittance of the fiberglass with concentrations of SiO_2 up to 65 weight percent. Higher concentrations of SiO_2 produces outstanding chemical stability, while the UV transmittance of glass composites gradually decreased with increasing Al_2O_3 content, and the UV transmittance of glass samples increased first and then decreased with increasing SiO2 content. A recent report from [4] indicated that iron oxidation state in or out of the produced glass has a significant effect on the boron-Eftimie, C-C. Udrea, M-A Melinescu, A-V. Filip / Study on fiber glasses with UV transmission oxygen structure of fiber glass and on the UV transmittance at a wavelength of 250 nm, the UV absorption coefficient of calcium oxide (CaO) being about four times greater than that of Ca_2O at 252 nm. Technical glasses for the UV region were also studied in an ample report of [5], who stated that, to achieve a higher UV transmission, it is necessary to optimize the Al2O3 content in the glass. Literature reports some patents dealing with fiberglass, claiming high UV transmission, like [6], with fiberglass with UV transmission of at least 85% at a UV wavelength of about 250 nm for a fiberglass sheet thickness of 3 mm. The report indicated the results of an investigation on UV-Vis transmission of some samples of fiberglass with low alkali Na_2O content and melting temperatures of 1500 °C, through the method of melt quenching. The X-ray diffraction was used to confirm feasible characteristics, and UV-Vis transmission to assess the light transmission down to 250 nm, which allows the studied glasses use in optical applications.

Materials and Methods

In this investigation, fiberglass was synthesized through melt quenching technique. The compositions of the synthesized glasses are presented in Table 1. The raw materials were silicon dioxide (SiO_2), sodium oxide (Na_2O), potassium oxide (K_2O), lithium oxide (Li_2O), zinc oxide (ZnO) and alumina (Al_2O_3). The compositions were chosen to have high concentrations of SiO_2 to lower the melting temperature, while Na_2O, K_2O and Li_2O lowered the viscosity of melts for a good fining process. Al_2O_3 and ZnO were added to increase the stability of glasses. The materials were weighed on an analytical balance and dry-

homogenized in a mortar for 20 minutes. The fiber glasses were melted at different temperatures between 1400 and 1600°C due to compositional differences and depending on the viscosity of the melts. The melting process was carried out in alumina crucibles into electric furnace and, the no. 3 glass melt had gas and water bubbles trapped even after a 3-hour firing. Casting of the 30 x 30 x 5 mm samples took place in a graphite form. The annealing temperatures were estimated based on melting temperatures, then established through dilatometry and the composites were annealed again in the oven with 1 hour at the annealing temperature specific for each glass sample, with 1°C/min decrease rate down to strain temperature, then the samples were left to cool in the annealing oven to the laboratory temperature. Density was measured using weighing balance and Archimedes' principle method. Thermal expansion and specific temperatures were obtained using a DIL402 PC dilatometer from NETZSCH, Germany with 3°/min rate, in air. Chemical stability was assessed measuring the conductivity of a solution made of water and grinded glass, at constant temperature, for 2 hours, using an AGILENT 3200C conductivity meter. The glass samples were grounded in a mortar, passed through two sieves with different mesh sizes of 25 and 50 μm. The closer the sieves mesh sizes are to each other, the less dispersed the grain size fraction between the two sieves will be and the more constant the average fraction size (i.e. its specific surface area) will be from one glass sample to another. From this fraction (1g) was weighed on the analytical weighing balance and then mixed with 50 ml of distilled water in a beaker. The mix was continuously stirred for 180 minutes at 27 °C and its electrical conductance was measured with the aid of the conductivity meter every minute for the first 5 minutes, then every 5 minutes for the remaining time. The conductance of distilled water was previously measured at the same temperature and was subtracted from all the glass-water mix measurement values. UV-Vis spectroscopy was carried out using a UV- spectrometer. Fiber glass samples were prepared and displayed in Table 1.

Table 1: Glass Sample Compositions

Samples	$Si0_2$	Al_2O_3	CaO	MgO	Na_2O	K_2O	Li_2O
A	50	8.0	18.5	4.6	0.3	0.2	7.3
B	55	6.5	16.5	4.0	5.6	1.6	6.5
C	60	3.0	15.5	3.5	7.8	2.8	5.8
D	65	4.0	14.0	3.0	8.5	3.0	5.0

M-A. Eftimie, C-C. Udrea, M-A Melinescu, A-V. Filip / Study on fiberglass samples with UV transmission 207
Glass samples were presented for UV-Vis analyses, and tested on a high-performance machine. The thickness of the samples was 3 mm. For XRD measurements to confirm the structural dynamics of the samples, a BRUKER D8 ADVANCE USA type X-ray diffractometer (Cukaα, λ= 1.54 Å) was used. The X-ray pattern was acquired at laboratory temperature, using a step of 0.05° and 5 s integration time, the scan being done between 15° and 70° (2θ range). ICDD powder Diffraction database was used for phase identification, Proton Induce X-Ray Emission (PIXE) and Rutherford Back Scattering (RBS) measurements were carried out with percent concentration error of between ± 0.00001 and 0.5.

The Scanning Electron Microscope (SEM) of Four Samples

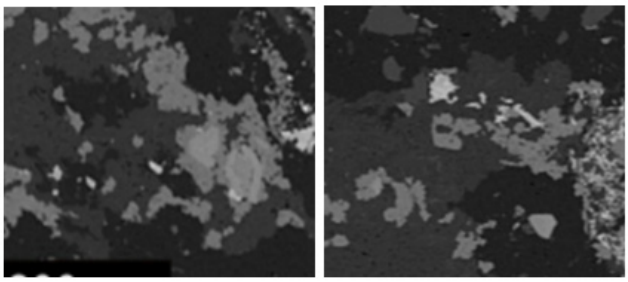

(a) Sample A (200μm) (b) Sample B (200μm)

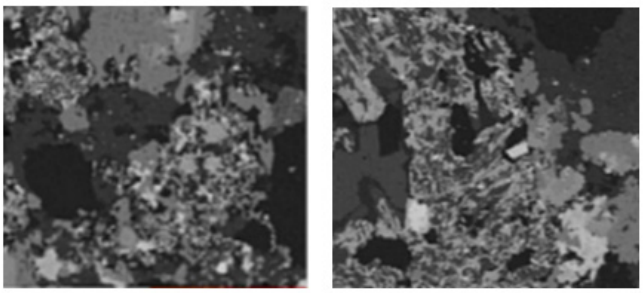

(c) Sample C (200μm) (d) Sample D (200μm)

Results and Discussion

Table 2: Thermal Properties of Glass Samples

Glass Samples	Thermal Expansion, α (10^6K^{-1})	Strain Temperature, Ts (°C)	Glass transition Temperature, Tg (°C)	Stress Temperature, Ts (°C)	Dilatometry Softening Temperature, Td (°C)
A	3.83	480	532	543	554
B	5.39	445	487	608	533
C	3.80	460	492	510	544
D	4.82	432	521	520	548

Table 3: Concentration of Elements in Sample A

S/N	Element/Symbol	% Conc.	% Conc Error	% LOD	Present
1	Oxygen (O)	20.11062	±0.027508	0.01497	Y
2	Sodium (Na)	5.497660	±0.215664	0.29829	Y
3	Magnesium (Mg)	4.23964	±0.165492	0.15065	Y
4	Aluminum (Al)	20.13075	±0.045969	0.01613	Y
5	Silicon (Si)	25.11359	±0.082875	0.02739	Y
6	Potassium (K)	7.08710	±0.008597	0.01600	Y
7	Calcium (Ca)	8.89213	±0.009712	0.00652	Y
8	Lithium (Li)	4.03139	±0.002882	0.00494	Y
	Total	95.1921			

Table 3 summarizes the elements, their percentage elemental concentrations, and the variation in concentration error of sample A. The level of significance was between 0.01 and 0.3, and the level of determination was in the range 0.00494 to 0.2983. The results showed that the oxygen and aluminium atoms have an equal elemental concentration of 20.0 percent each, with an empirical concentration error of approximately ±0.027508 to ±0.04597. Sodium, calcium, and silicon were determined at approximately 5.5, 8.89, and 25.0 percent concentrations, respectively, with levels of significance between 0.01 and 0.3. It implies there was an increase in the level of determination before highly concentrated elements were determined.

Table 4: Concentration of Elements in Sample B

S/N	Element/Symbol	% Conc.	% Conc Error	% LOD	Present
1	Oxygen (O)	15.14062	±0.027508	0.01497	Y
2	Sodium (Na)	14.57668	±0.215664	0.29829	Y
3	Magnesium (Mg)	5.23964	±0.165492	0.15065	Y
4	Aluminum (Al)	18.73075	±0.045969	0.01613	Y
5	Silicon (Si)	27.11359	±0.082875	0.02739	Y
6	Potassium (K)	6.08710	±0.008597	0.01600	Y
7	Calcium (Ca)	9.59213	±0.009712	0.00652	Y
8	Lithium (Li)	3.03139	±0.002882	0.00494	Y
	Total	99.5826			

Table 4 indicates the elements, percentage elemental concentrations, and concentration error variation of sample B. The level of significance was between 0.01 and 0.3, and the level of determination was in the range 0.00494 to 0.2983. The results showed that the silicon element has a concentration of 27.1 percent, and the empirical concentration error is ± 0.082875 approximately. Oxygen, sodium, calcium, and potassium were determined at approximately 15.14, 14.57, 9.59, and 6.08 percent concentrations, respectively, with levels of significance between 0.01 and 0.30. It signifies there was an increase in the level of significance before highly concentrated elements were observed.

Table 5: Concentration of Elements in Sample C.

S/N	Element/Symbol	% Conc.	% Conc Error	% LOD	Present
1	Oxygen (O)	15.34062	±0.027508	0.01497	Y
2	Sodium (Na)	13.97668	±0.215664	0.29829	Y
3	Magnesium (Mg)	5.03964	±0.165492	0.15065	Y
4	Aluminum (Al)	16.81075	±0.045969	0.01613	Y
5	Silicon (Si)	28.11359	±0.082875	0.02739	Y
6	Potassium (K)	1.08710	±0.008597	0.01600	Y
7	Calcium (Ca)	10.59213	±0.009712	0.00652	Y
8	Lithium (Li)	1.53139	±0.002882	0.00494	Y
	Total	95.484516			

In Table 5 for sample C, it was observed that the concentration of aluminium is thrice that of magnesium. Silicon was also twice that of the concentration of sodium. Silicon takes the highest concentration elements with 28.1 percent, 0.01 level of significance, 0.027 level of determination, and ± 0.082875 error concentration. It entails the highest concentration of an element at a low level of determination and small error concentration. Sodium, oxygen, and calcium concentrations in the range 14.98 - 16.00 percent were determined with levels of significance between 0.01 and 0.3. These were determined at a low level of determination and between low and high error concentrations, ± 0.002882 and ± 0.215664. This sample was noted to be close to 100.0 percent elemental concentration.

Table 6: Concentration of Elements in Sample D

S/N	Element/Symbol	% Conc.	% Conc Error	% LOD	Present
1	Oxygen (O)	15.34062	±0.027508	0.01497	Y
2	Sodium (Na)	14.97668	±0.215664	0.29829	Y
3	Magnesium (Mg)	7.41964	±0.165492	0.15065	Y
4	Aluminum (Al)	15.94075	±0.045969	0.01613	Y
5	Silicon (Si)	29.61359	±0.082875	0.02739	Y
6	Potassium (K)	4.08710	±0.008597	0.01600	Y
7	Calcium (Ca)	10.59213	±0.009712	0.00652	Y
8	Lithium (Li)	1.23139	±0.002882	0.00494	Y
	Total	99.17486			

In Table 6 for sample D, silicon takes the highest concentration element with 29.6 percent, 0.01 level of significance, 0.027 level of determination, and ±0.082875 error concentration. It depicts the highest concentration of the element at a low level of determination and small error concentration. Sodium, oxygen, and calcium concentrations in the range 10.59 - 16.00 percent were sustained with levels of significance between 0.01 and 0.3. These were determined at a low level of determination, and between low and high error concentrations, ± 0.009712 and ± 0.215664. This sample was revealed to be very close to 100.0 percent elemental concentration. Y = Yes, LOD = Level of Determination, dash = not certain, and Oxygen was obtained from RBS analysis, and other elements are from PIXE. Air trap and moisture constitute the remaining percentage.

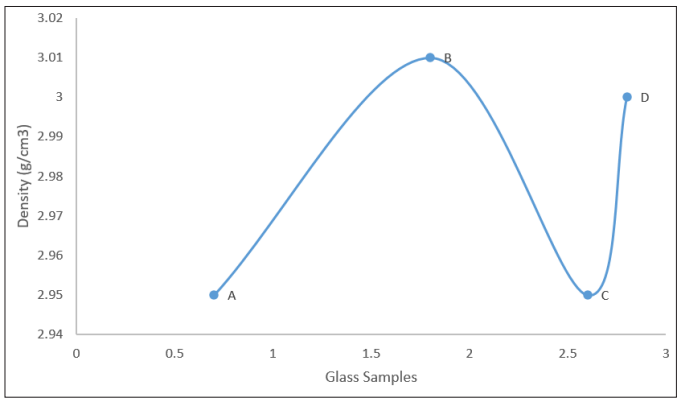

Figure 1: The Glass Sample Density

In Figure 1, the densities of fiberglass samples were obtained. The densities obtained for fiberglass samples have closer values, as depicted in Figure 1 above. However, glass samples A and C have the lower density values compared to the other samples. This was because of the chemical composition of the glass samples A and C. Unlike the other two samples, where the mass percentage of Al_2O_3 varies between 4.0 and 6.5 %, sample C contains a much lower mass percentage of Al_2O_3. Since the molecular mass of alumina is 102 g/mol, a lower percentage of Al_2O_3 determines the density of the glass. On the other hand, glass sample A had a much higher number of gas bubbles compared to the other two samples, which, for the same volume, decreases the mass and, therefore, the density of the sample, which becomes apparent density for this sample, due to the trapped bubbles.

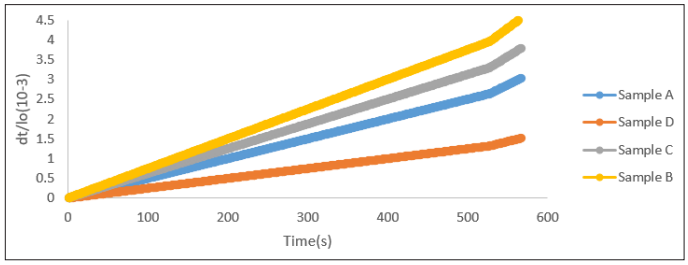

Figure 2: The thermal expansion curves of the samples

The thermal expansion curve measured by dilatometry in Figure 2 gives important properties: the coefficient of thermal expansion (α), the glass structural transformation temperature or glass transition temperature (Tg), annealing and strain temperature (Ta and Ts), and the dilatometry softening temperature (Td), as presented in Table 2. From the thermal expansion curves, the experimentally developed samples had very low coefficients of thermal expansion for the fiberglass samples, which makes the glasses capable of resisting thermal shocks as well as low and close glass transition and dilatometry softening temperatures, which correlate with the low content of alkali oxide. Chemical reactions with glass surfaces are those induced by weathering, depletion, and absorption. Glass sample no. 208 M-A. Eftimie, C-C. Udrea, M-A Melinescu, A-V. Filip / Study on fiberglass with UV transmission is displayed in Table 2. Thermal properties of the glass samples, glass sample thermal expansion, $\boldsymbol{\alpha 20\ 300}$ x 10^6, [K^{-1}] Strain temperature, Ts, °C, Glass transition temperature, Tg, °C, Strain temperature, Ts, °C, a dilatometry softening temperature, Td, °C.

The composition of the glass, the method of fabrication, and the coating conditions decide to what extent these chemical attacks are technically significant [7]. For light applications, glass must be resistant to different chemical solutions so that multiple reflections can take place without the risk of damaging the glass or equipment. In addition, acid attack is of vital relevance both in laboratories and in chemical technology. The assessment of the dynamics of the water attack process on glass is very necessary. The conductivity method provides a good report. This measures the variation of the electrical conductance of a suspension of glass powder in water as a function of time, and other temperatures, the amount of glass powder and its specific surface area, and the content of water in the suspension. The method has the advantage of measuring the dynamics of the process of attack of the glass by the water, revealing whether this process stops over time (stabilization process) or evolves continuously without stopping (degradation process). The results are presented in Figure 3. The hydrolytic stability of the analyzed samples shows that they are chemically stable, with conductivities below 20 µS/cm. Sample A has the highest conductivity value, which means that it had a rapid release of ions in the first hour and then it stabilizes. Samples B, C, and D show lower conductivity values, have a slow but quasi-particle release of ions, even after two hours of analysis. The lower conductivity means a very good chemical stability, which makes the glasses chemically resistant to various materials and liquids, as well as to different light applications.

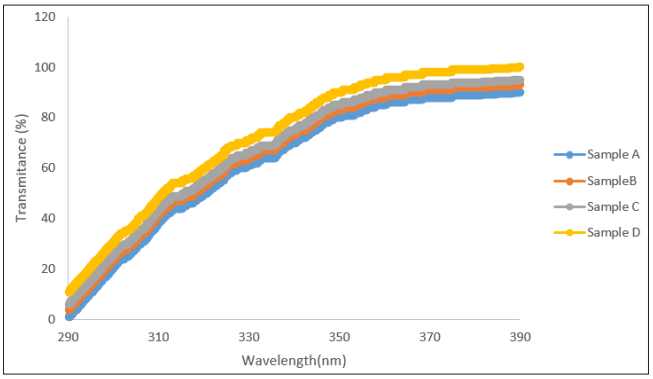

Figure 3: UV-Vis transmission of samples

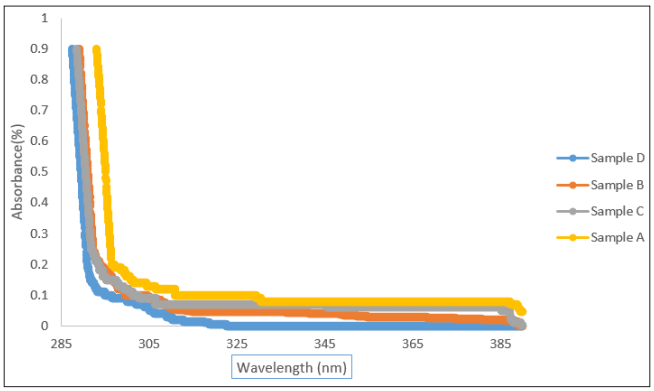

Figure 4: UV-Vis Absorbance of samples

The UV-Visible absorption of glasses is useful for studying optical properties, electronic transitions, and bonding nature in glass lattices due to the optical band gap of various glass contents. Moreover, electronic transitions induced the optical band structure of glass materials. The different types of electronic transitions between the valence band and the conduction band are direct and indirect transitions [8, 9 & 10]. The results presented in Figure 4 indicate that glass samples A, B, C, and D showed transmission in the UV region, having a maximum transmission of ~ 80 to 90 % at 350 nm wavelength in the visible range. Samples A, B, C, and D showed a transmission of 25 to 35 % at 300 nm wavelength in the UV range. Samples A, B, C, and D have a maximum transmission of 90 to 99.9 % at ~ 390 nm wavelength in the visible range. The obtained values in the UV region are quite good, considering the thickness (literature data uses 2- or 3-mm thick samples), and can be associated with the structure of the glass through the presence of bubbles and water, and with the composition (sodium oxides and aluminum oxide), which decreases the UV transmission.

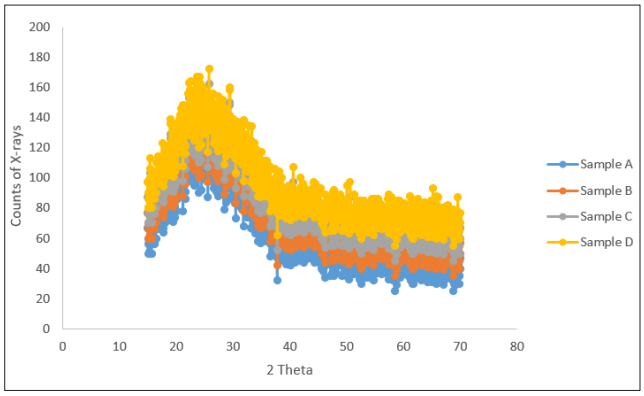

Figure 5: XRD spectra for glass samples

The XRD spectra pattern was displayed in Figure 5. Fiberglass samples present a wide scope equivalent to the glassy phase in the system for every sample. The XRD pattern shows only one broad diffraction band with a large width for each sample, with one peak associated with any crystalline phase, verifying the amorphous nature of the glass samples. The width of the diffraction band increases as the silicon dioxide content increases. The residual noise increased for each sample, which proves the amorphous nature of the processed fiberglass and a study on fiberglass with UV transmission.

Conclusions

The new fiberglass has been obtained with good transmission of electromagnetic radiation in the UV-Vis region, low thermal expansion coefficient, and high chemical stability. They are proposed for various applications such as UV lamps, photomultipliers, spectrophotometers etc. The density of the samples showed similar values for the four samples analyzed. The hydrolytic stability of the samples revealed that they are very stable. From the thermal expansion the processed samples had low expansion coefficients, between $20x10^{-7}$ and $40v10^{-7}$ K^{-1}.

In the UV-Vis transmission, the samples have excellent transmittance. In the visible range, with a maximum transmission of 90-99 percent at wavelengths of 350-390 nm, making them suitable materials for applications of visible light and in the ultraviolet region, considering the 3 mm thickness of the samples. The morphology of the glasses that contain some air and water bubbles, and the alkali oxides that lower the transmittance of UV light in the processed glass samples. By the presence of a specific peak in the spectrum, XRD analysis also showed that the fiberglass samples did not crystallize; the presence of a wide band full-width half-maximum for each sample verifies the amorphous nature of the processed glass.

References

1. Hegazy DA, AwdAllah MM, Alshahrani H, Sebaey TA, Abd El-baky MA (2025) Effect of alumina nanoparticles on collapse behavior and energy absorption of laterally loaded glass/epoxy composite tubes. Polym Compos 46: 1067-1079.
2. Junaedi H, Khan T, Abd-Elaziem W, Sebaey TA, Akkad K (2025) Optimization of circular hole patterns on crashworthiness of polyurethane foam-filled CFRP rectangular tubes. Results Eng 26: 104805.
3. Ashwin NR, Musa A, Ranjit JS, Yasser EI, Anant LM, et al. (2024) Investigating crumb rubber-modified geopolymer composites derived from steel slag for enhanced thermal performance. Eng Sci Technol Int J 59: 101880.
4. Li C, Liao H, Gao H, Cheng F (2024) Enhancing interface compatibility in high-filled coal gangue/polyethylene composites through silane coupling agent-mediated interface modification. Compos Sci Technol 251: 110546.
5. Liu Z, Tao S, Dong X, Jie Z, Libing L, et al. (2024) Effect of seawater corrosion on the mechanical properties of basalt fiber reinforced polymer composites modified by silane coupling agent KH560 and carboxylated carbon nanotubes. Mater Today Commun 40: 109753.
6. Hu Y, Liu Y, Zheng S, Kang W (2024) Progress in application of silane coupling agent for clay modification to flame retardant polymer. Molecules 29: 4143.
7. AwdAllah MM, AbdEl-baky MA, Alshahrani H, Sebaey TA, Hegazy DA (2023) Energy absorption capability of laterally loaded glass/epoxy tubular components containing halloysite nanotubes. J Compos Mater 57: 4307-4325.
8. Shaker K, Adnan M, Nawab Y, Umair M, Jabbar M, et al. (2023) Mechanical performance of glass/epoxy composites loaded with silane-treated aluminum hydroxide fillers. Polymers 15: 3514.
9. Patel BS, Emami S, Gabil H (2022) Thermal and mechanical properties of blends and composites from LDPE and date pits particles. J Compos Mater 40: 80-89.
10. uradia A, Norshahida S, Sopyan I, Zahurin H (2021) Effect of fibre length variation on coir fibre reinforced cement-albumen composite. IIUM Eng J 12: 63-75.